# Supporting Information

**Autonomous Light Management in Flexible Photoelectrochromic Films Integrating High Performance Silicon Solar Microcells**

*Maggie M. Potter,[†] Mikayla A. Yoder,[†] Aaron Petronico, Sean E. Lehman, Bruno G. Nicolau, Michael J. Enright, Megan Phelan, Junwen He, Harry A. Atwater, Ralph G. Nuzzo**

Ms. M. M. Potter
Department of Chemical and Biomolecular Engineering, University of Illinois at Urbana-Champaign, Urbana, Illinois 61801, USA.

Dr. M. A. Yoder, Dr. A. Petronico, Dr. S. E. Lehman, Dr. B. G. Nicolau, Dr. M. J. Enright, Dr. J. He, Prof. R. G. Nuzzo
School of Chemical Sciences, University of Illinois at Urbana-Champaign, Urbana, Illinois 61801 USA

Ms. M. Phelan, Prof. H. A. Atwater
Thomas J. Watson Laboratories of Applied Physics, California Institute of Technology, Pasadena, CA 91125, USA

Prof. R. G. Nuzzo
Surface and Corrosion Science, School of Engineering Sciences in Chemistry, Biotechnology and Health, KTH Royal Institute of Technology, Drottning Kristinasväg 51, 100 44 Stockholm, Sweden

*E-mail: r-nuzzo@illinois.edu

[†]Authors contributed equally to the work.

## 1. Experimental Methods

### 1.1. Electrochromic Materials Synthesis and Assembly

Both metal oxide films are prepared via sol-gel methods. They are spin-coated on a substrate, either glass or ITO-coated glass followed by thermal annealing, which expels residual solvent as well as structurally reorganizes the metal oxide layers. Following preparation of a gel-based lithium electrolyte, the device is assembled; a schematic of this configuration can be seen in **Figure 2a**. Details of the syntheses and device assembly are described below.

#### *1.1.1. Tungsten (VI) Oxide Synthesis*

To prepare $WO_3$ thin films, 0.25 g of $WOCl_4$ is combined with 5 mL isopropanol (IPA) and stirred overnight until the solution is homogenous and clear.[1-2] The $WOCl_4$ powder is weighed in a glovebox with $O_2$ concentration < 3 ppm and transferred to a septum-sealed flask; then the IPA is added with a syringe and the solution is stirred overnight. The homogenous, clear solution is spin-coated onto the desired substrate at 1200 rpm, allowing ambient room humidity to hydrolyze the film. The film is then annealed in a tube furnace open to air at 150°C for 1 hour to drive off the residual solvent. This process is repeated (spin-coating and annealing) twice more, for a total of three layers. The total layer thickness is approximately 207 nm, as determined through optical profilometry.

#### *1.1.2. Vanadium (V) Oxide Synthesis*

The $V_2O_5$ films are also prepared from the sequential hydrolysis and condensation of $VO(OC_3H_7)_3$, following a modified procedure by Nilgün Özer.[3-4] IPA is added as a solvent, acetic acid as a catalyst, and water to hydrolyze the reaction. We found that using air humidity

to hydrolyze the isopropoxide is not consistent and therefore added water in a 1:1 mole ratio with the precursor. The solution is spin-coated onto the desired substrate at 1800 rpm and annealed in a tube furnace at 300 °C under pure $O_2$ flow (~0.2 slpm) to promote condensation via dehydration as well as drive off residual solvent and water from the hydrolysis protocol. A total of three layers were deposited and heat treated to give a thickness of approximately 166 nm as determined through optical profilometry.

*1.1.3. Preparation of Gel Electrolytes*

The gel electrolyte is first prepared by making a 1 M lithium bis(trifluoromethanesulfonyl)imide (LiTFSI) solution in propylene carbonate (PC) in the glovebox. After the salt is dissolved, 35 wt.% poly(methyl methacrylate) (PMMA, $M_W$ = 120,000, Sigma Aldrich) is added while the solution is vigorously stirred. To completely homogenize the gel, the solution is manually stirred and left on low heat. The solution is kept in a dry box to prevent the LiTFSI from absorbing water.

*1.1.4. Assembly of the Electrochromic Film*

The prepared gel electrolyte is first spread over a $V_2O_5$ film on ITO/glass and degassed for >12 hours. Concurrently, $WO_3$ films are pre-lithiated in the glovebox using 0.1 M LiTFSI in PC and a lithium metal counter and reference electrode. The $WO_3$ film is reduced at 2.1 V vs. $Li/Li^+$ to switch the film to its colored state. The film is then rinsed with PC, dried, and taken out of the glovebox. To obtain reproducible thicknesses of the gel electrolyte, soda lime glass beads with diameters of 100 μm (SPI, Product 2720-AB) were used as spacers. These were placed in the corners of the degassed gel electrolyte on $V_2O_5$ and the reduced $WO_3$ film was placed on top.

This assembly was then brought into the glovebox and encapsulated with NOA61 on each edge of the glass. The NOA61 was cured under UV (365 nm, 4 W) for 40 minutes.

*1.1.5. Assembly/Testing with Corning® Willow® Glass*

The electrochromic materials (i.e., metal oxide films and gel electrolyte) were prepared as previously described and the device was assembled on 100-micron thick Corning® Willow® glass coated with ITO (185 nm, sheet resistance of 15-30 ohms per square) as deposited by THINFILMS, Incorporated. A layer of 0.010"-thick polyethylene terephthalate (PET) was adhered to the Corning® Willow® glass using NOA61 on the front and back of the device to facilitate device assembly and encapsulation. A dynamic mechanical analyzer (DMA) was used to apply and remove a force upon the device with the 3-point flexural test setup. For compatibility with the 3-point flexural test setup, active device area was enlarged to 12 mm x 20 mm.

**1.2. Materials Characterization**

*1.2.1. X-ray Characterization of Metal Oxide Films*

X-ray photoelectron spectra were collected using a Kratos AXIS Ultra spectrometer equipped with a monochromatic Al Kα (1486.6 eV) X-ray source. High resolution spectra were collected with a pass energy of 40 eV and at a resolution/step size of 0.1 eV. Data was processed and analyzed in Origin 9.1. Spectral peaks were referenced to the adventitious C 1s peak at 284.8 eV. A Shirley or Tougaard background was used to baseline correct the spectra. Curve-fitting was carried out using a Gaussian lineshape function for analysis of the integrated peak areas.

A PANalytical X'Pert instrument equipped with a Cu Kα (1.54 Å) source and Ni filter was

used to collect X-ray diffraction patterns of the deposited metal oxide thin films. The generator voltage and tube current were set to 40 kV and 40 mA, respectively. High resolution measurements were obtained by collecting data from 10-100° 2θ using a 0.05° step size. Samples were immobilized by taping them directly onto the sample stage with Scotch tape for positioning and measurement. Data was collected using a point-parallel plate geometry.

*1.2.2. Rheology of PMMA-PC-LiTFSI*

Rheological measurements were carried out on a DHR-3 rheometer (TA Instruments) using a parallel-plate geometry with a diameter of 20 mm with Peltier temperature control. The gap between plates was continuously varied to maintain a force of 0 ± 0.1 N normal to the direction of flow. The rotational shear rates varied linearly and the temperature was controlled to be constant at 25°C for the duration of the experiments. 600 grit silicon carbide paper with an adhesive backing was implemented to prevent slip.

*1.2.3. UV-Visible Spectroscopy*

Transmittance measurements were taken on an Agilent Cary Series UV-Vis-NIR Spectrophotometer from 300 – 2000 nm using a diffuse reflectance accessory, with a data interval of 1.0 nm and a scan rate of 600 nm/min. A baseline was taken to determine 100 %T with the corresponding substrate; for the EC device on ITO/glass from 300 - 1400 nm, the blank consisted of two pieces of ITO/glass sandwiched together with an air gap determined by a 100 μm PDMS spacer with a hole punched in the middle. At wavelengths 1400 – 2000 nm, the blank consisted of two pieces of glass (sans ITO) sandwiched together with an air gap determined by a 100 μm PDMS spacer with a hole punched in the middle. To correct for Fresnel losses associated

with the air gap in both blanks, the reflection losses at the interior interfaces only were calculated by wavelength using tabulated refractive index data for ITO[5] and glass[6] assuming normal incidence ($R = \left|\frac{n_1 - n_2}{n_1 + n_2}\right|^2$), and the resulting % loss was added back into the 100% T reference spectra prior to application of the standard baseline correction to the raw recorded sample data [**Figure S5(a-f)**].

*1.2.4. Cyclic Voltammetry*

A CH Instruments electrochemical workstation was used to perform cyclic voltammetry with a three electrode setup. Each metal oxide was cycled from 2.1 – 4.0 V vs. $Li/Li^+$ using lithium metal as a reference and counter electrode. $WO_3$ films were cycled at 50 mV $s^{-1}$ in 0.1 M $LiClO_4$ in PC and $V_2O_5$ films were cycled at 1 mV $s^{-1}$ in 1 M $LiClO_4$ in PC. Voltammetry with the gel electrolyte was also performed with each metal oxide film using the same system above with a scan rate of 1 mV $s^{-1}$ or 0.1 mV $s^{-1}$.

*1.2.5. Electrical Impedance Spectroscopy*

The gel electrolyte was prepared and spread into a hollow, cylindrical PDMS mold on top of a steel electrode. A second electrode was placed on top and the assembly was put into a Swagelok cell for measurements. Potentiostatic electrochemical impedance spectroscopy was conducted using a Biologic (Seyssinet-Pariset) SP150 potentiostat/galvanostat. Scans were run with a frequency range of 1.0 MHz to 100 mHz at 0 V vs. working electrode and with a perturbation amplitude of 20 mV. The bulk resistance of the polymer electrolyte was calculated by finding the intercept of the sloped curves [**Figure S4(a-b)**] with the real axis (Z') of the Nyquist plot, as opposed to utilizing the fit of an equivalent circle. This procedure is adapted

from Goodenough *et al.*[7] and has been commonly used[8-10] to determine the resistance of bulk electrolyte in gel polymer electrolytes in the past. In the case of gel electrolytes, it has been posited that the electrode electrolyte interface presents quite fast ionic mobility, resulting in very low capacitance effects in the higher frequency regions and thus, the usual semi-circle in the high frequency region of the Nyquist plot is not present.

### 1.3. Silicon Solar Microcell Fabrication and Testing

The details of the fabrication of silicon solar microcells can be found in Reference 11. Deterministic assembly is used to transfer print the μ-cells onto desired substrates. The μ-cells are planarized with NOA61 and interconnected via evaporated Cr/Au with a shadow mask connecting one, two, or three μ-cells in series. *I-V* data was collected with a full-spectrum solar simulator (Model 91192, Oriel) with a source meter (Model 2400, Keithley). Further details on the fabrication, transfer printing, and testing are explained in Reference 11.

### 1.4. Electrochromic Device Characterization

Cycling of the assembled EC device was performed on the same UV-Vis-NIR spectrophotometer as described above. A source meter (Model 2400, Keithley) was used to switch the device between a positive and negative bias. The EC device was connected with copper tape on either electrode, connected to leads from the source meter. The spectrophotometer continuously monitored transmission at 600, 1200, and 1600 nm during cycling with a spectral band width (SBW) of 1 nm and average time of 0.1 sec.

### 1.5. Photoelectrochromic Device Characterization

The modulation of transmission of the EC device powered by the Si μ-cells was monitored with the same setup above. The Si μ-cells were irradiated with a full-spectrum simulator (Model 94021, Oriel) calibrated to 1 sun intensity. Intensity was modulated with neutral density (ND) filters (unmounted Ø25 UV fused silica reflective ND [OD = 0.1, 0.3, and 0.6] filters, Thorlabs) to simulate 0.79, 0.5, and 0.25 sun irradiation.

**References**


1. Krings, L. H. M.; Talen, W. Wet Chemical Preparation and Characterization of Electrochromic $WO_3$. *Sol. Energy Mater. Sol. Cells* **1998,** *54* (1), 27-37.
2. Caruso, T.; Castriota, M.; Policicchio, A.; Fasanella, A.; De Santo, M. P.; Ciuchi, F.; Desiderio, G.; La Rosa, S.; Rudolf, P.; Agostino, R. G.; Cazzanelli, E. Thermally Induced Evolution of Sol–Gel Grown $WO_3$ Films on ITO/Glass Substrates. *Appl. Surf. Sci.* **2014,** *297* (Supplement C), 195-204.
3. Özer, N. Electrochemical Properties of Sol-Gel Deposited Vanadium Pentoxide Films. *Thin Solid Films* **1997,** *305* (1), 80-87.
4. Özer, N.; Sabuncu, S.; Cronin, J. Electrochromic Properties of Sol-Gel Deposited Ti-Doped Vanadium Oxide Film. *Thin Solid Films* **1999,** *338* (1), 201-206.
5. Holman, Z. C.; Filipič, M.; Descoeudres, A.; Wolf, S. D.; Smole, F.; Topič, M.; Ballif, C. Infrared Light Management in High-Efficiency Silicon Heterojunction and Rear-Passivated Solar Cells. *J. Appl. Phys.* **2013,** *113* (1), 013107.
6. Rubin, M. Optical Properties of Soda Lime Silica Glasses. *Sol. Energy Mater.* **1985,** *12* (4), 275-288.
7. Gao, H.; Guo, B.; Song, J.; Park, K.; Goodenough, J. B. A Composite Gel–Polymer/Glass–Fiber Electrolyte for Sodium-Ion Batteries. *Adv. Energy Mater.* **2015,** *5* (9), 1402235.
8. Appetecchi, G. B.; Croce, F.; De Paolis, A.; Scrosati, B. A Poly(Vinylidene Fluoride)-Based Gel Electrolyte Membrane for Lithium Batteries. *J. Electroanal. Chem.* **1999,** *463* (2), 248-252.
9. Panero, S.; Scrosati, B. Gelification of Liquid–Polymer Systems: A Valid Approach for the Development of Various Types of Polymer Electrolyte Membranes. *J. Power Sources* **2000,** *90* (1), 13-19.
10. Petronico, A.; Moneypenny, T. P.; Nicolau, B. G.; Moore, J. S.; Nuzzo, R. G.; Gewirth, A. A. Solid–Liquid Lithium Electrolyte Nanocomposites Derived from Porous Molecular Cages. *J. Am. Chem. Soc.* **2018,** *140* (24), 7504-7509.
11. Yoder, M. A.; Yao, Y.; He, J.; Nuzzo, R. G. Optimization of Photon and Electron Collection Efficiencies in Silicon Solar Microcells for Use in Concentration-Based Photovoltaic Systems. *Adv. Mater. Technol.* **2017,** *2* (11), 1-9.

**Table S1.** Injected charge during CV processes in **Figure 3f** and **Figure 3i** at 1 mV/s, and in **Figure S4** at 0.1 mV/s.

| Oxide | Film Layers | Thickness | CV Scan Rate (mV/s) | Charge Inserted ($mC/cm^2$) |
|---|---|---|---|---|
| $WO_3$ | 3 | 230 | 0.1 | 9.5 |
| $V_2O_5$ | 3 | 166 | 0.1 | 12.5 |
| $WO_3$ | 3 | 230 | 1 | 24.3 |
| $V_2O_5$ | 12 | 268 | 1 | 43.0 |

**Table S2.** EC performance before and after bending.

| Condition | Coloration Time (sec) | Bleaching Time (sec) | $\Delta T_{max}$ (%) | Coloration Efficiency ($cm^2\ C^{-1}$) |
|---|---|---|---|---|
| **Before Bending** | 27.5 | 34.1 | 28.2 | 51.9 |
| **After Bending** | 23.4 | 28.6 | 27.8 | 48.6 |
| **Change [%]** | 15.0 | 16.0 | 1.3 | 6.2 |

**SI Figure Captions**

**Figure S1.** Fits for XPS data of (a) $WO_3$ films and (b) $V_2O_5$ films.

**Figure S2.** Cyclic voltammetry performed with liquid electrolyte ($LiClO_4$ /PC) and with a lithium metal counter/reference electrode of (a) $WO_3$ and (b) $V_2O_5$.

**Figure S3.** Cyclic voltammetry performed with the gel electrolyte (35 wt.% PMMA/PC) at a scan rate of 0.1 mV/s for the purpose of balancing the EC device.

**Figure S4.** Characterization of the gel electrolyte. (a, b) Impedance spectroscopy of a (a) 30 wt.% and (b) 35 wt.% PMMA gel electrolyte. (c) Transmission of the 35 wt.% PMMA gel electrolyte. (d) Stability window of the 30 wt.% (black) and 35 wt.% (red) PMMA gel electrolyte.

**Figure S5.** Detailed description of 100% T reference blanks and corrections to reference spectra for Fresnel losses. (a) Schematic of ITO-based blank and associated Fresnel losses at interior air gap interfaces. (b) Schematic of air-based blank and associated Fresnel losses at interior air gap interfaces. (c) 100% T reference spectrum of ITO-based blank before and after correction for Fresnel losses. (d) 100% T reference spectrum of air-based blank before and after correction for Fresnel losses. (e) Example of EC device data with and without correction for Fresnel losses in the 100% T reference spectrum for the ITO-based blank. (e) Example of EC device data with and without correction for Fresnel losses in the 100% T reference spectrum for the air-based blank.

**Figure S6.** EC device transmission modulation with air-based blank used for the 100% T reference spectrum.

**Figure S7.** (a) Transmission of ITO on glass (sans correction for Fresnel reflection) with air as the 100% T reference spectrum. (b-d) EC device cycling at each bias monitored at (b) 600 nm (**Figure S5c** corrected 100% T reference), (c) 1000 nm (**Figure S5c** corrected 100% T reference), and (d) 1600 nm (**Figure S5d** corrected 100% T reference).

**Figure S8.** Transmission of (a) $WO_3$ and (b) $V_2O_5$ films in their bleached (red) and absorptive (blue) states. ITO/glass was used as the 100% T reference spectrum (**Figure S7a**).

**Figure S9.** (a) Magnitude of injected charge for coloration and bleaching over 10 cycles for 0.5, 1.0, and 1.5 V (blue, red, and black, respectively). (b-c) Integration of current for bleaching (b) and coloration (c). (d) Charge obtained for integration of the current at different time intervals.

**Figure S10.** Bias holds for bleached (solid lines) and colored (dashed lines) of the EC device monitored at (a) 1000 nm and (b) 1600 nm. The green dashed line indicates when the bias was removed.

**Figure S11.** (a) *J-V* curves for Si μ-cells with their contacts facing upwards (red) and downwards (blue) with an optical image of an array in the inset. (b) *J-V* curves for one and two Si μ-cells in series. (c) *J-V* curves for two Si μ-cells in series under varying irradiation. (d) Modeling results for expected transmission through the colored window with one μ-cell (blue), two μ-cells (red) or three μ-cells (black) in series.

**Figure S12.** (a) Dependence of $J_{SC}$ on waveguide area. (b) Calculated switching times for increased geometric gain. (c-d) Calculated switching times for a device with equal waveguide and EC area (c) without and (d) with concentration in the form of an LSC.

**Figure S13.** (a-b) Bias holds for the PEC device monitored at 600 nm in the (a) absorptive and (b) bleached states for 1 sun (black), 0.75 suns (red), 0.5 suns (blue), and 0.25 suns (pink). Dashed lines correspond to when the Si μ-cell was disconnected from the EC device. (c) Full spectrum modulation for each intensity. (d-e) Transmission at 600 nm after biasing the EC device for 3 minutes with two Si μ-cells in series for (d) bleaching and (e) coloration.

**Figure S14.** Linear correlation between voltage and injected charge used to calculate switching times under concentration.

**Figure S15.** (a) PV component of PEC device prepared on a PET substrate. (b) PEC device prototype on flexible substrates.

**Figure S16.** Force-displacement curves during bending cycles of the EC device.

**Figure S1**

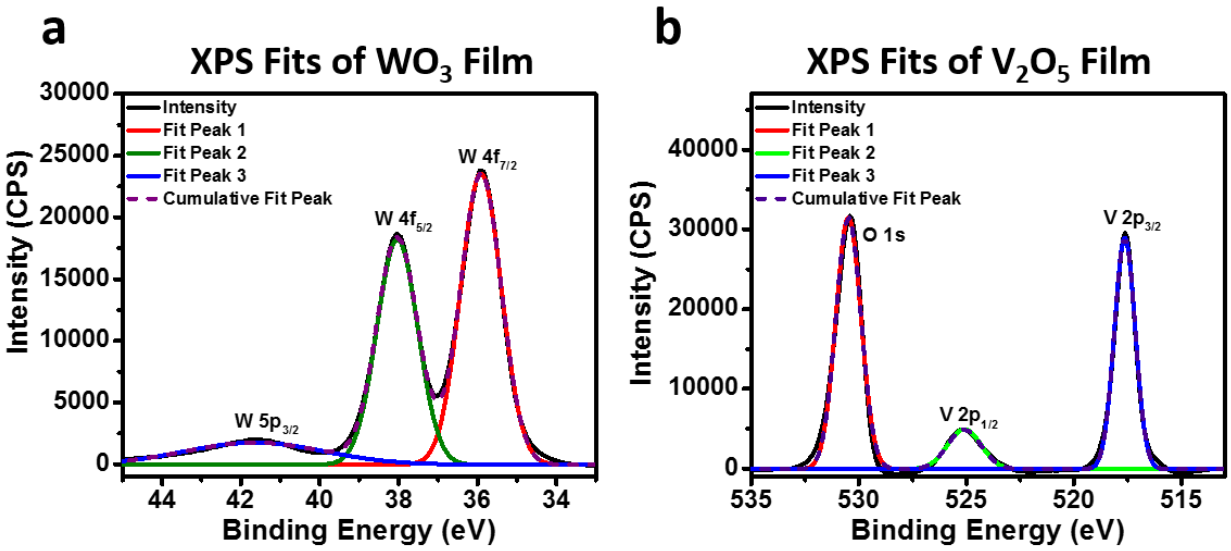
a
XPS Fits of $WO_3$ Film
Intensity
Fit Peak 1
Fit Peak 2
Fit Peak 3
Cumulative Fit Peak
W $4f_{7/2}$
W $4f_{5/2}$
W $5p_{3/2}$
Intensity (CPS)
Binding Energy (eV)
b
XPS Fits of $V_2O_5$ Film
O 1s
V $2p_{3/2}$
V $2p_{1/2}$

**Figure S2**

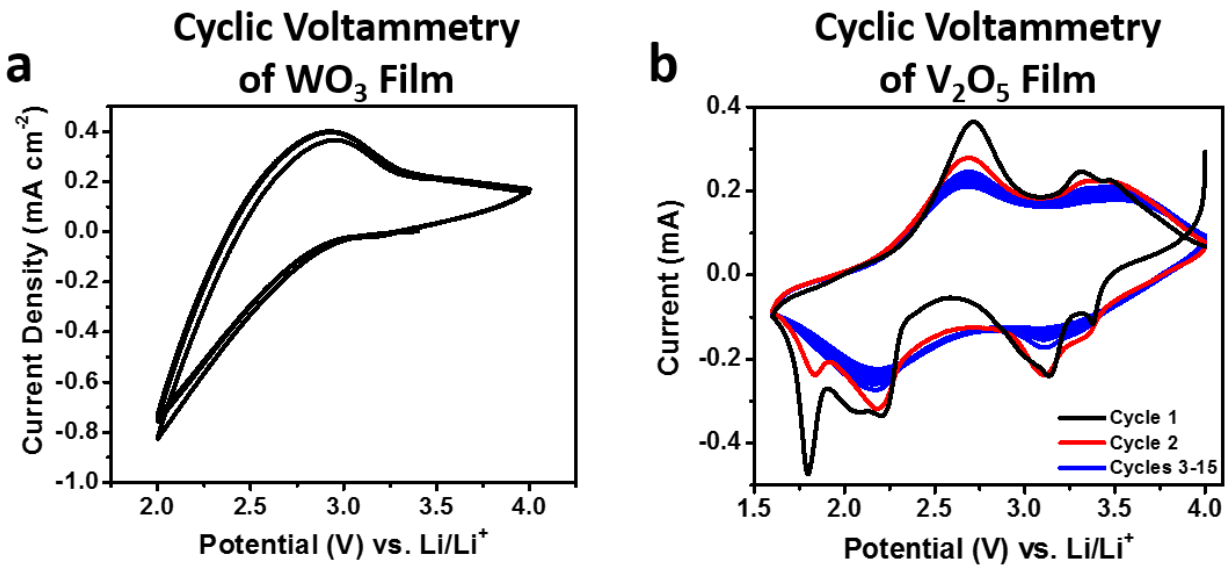
a
Cyclic Voltammetry
of $WO_3$ Film
Current Density (mA $cm^{-2}$)
0.4
0.2
0.0
-0.2
-0.4
-0.6
-0.8
-1.0
2.0
2.5
3.0
3.5
4.0
Potential (V) vs. $Li/Li^+$
b
Cyclic Voltammetry
of $V_2O_5$ Film
Current (mA)
0.4
0.2
0.0
-0.2
-0.4
1.5
2.0
2.5
3.0
3.5
4.0
Potential (V) vs. $Li/Li^+$
Cycle 1
Cycle 2
Cycles 3-15

**Figure S3**

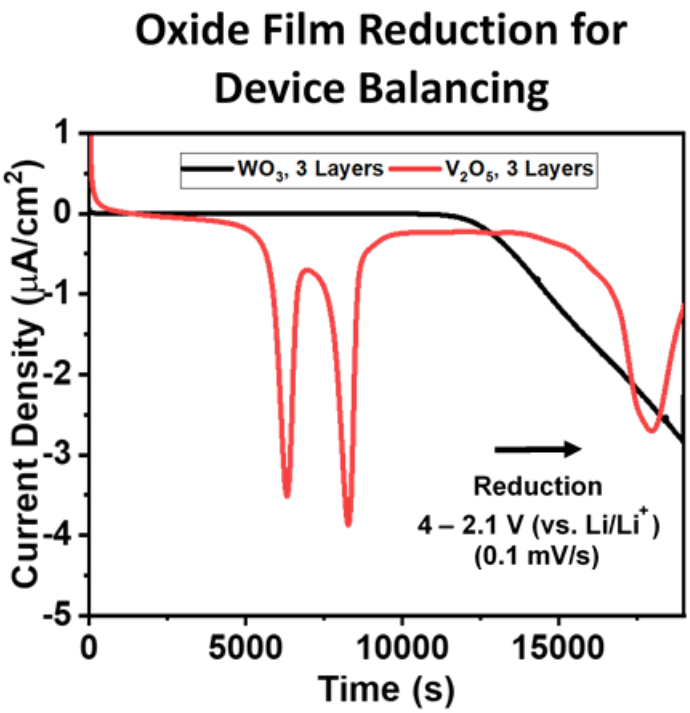
Oxide Film Reduction for Device Balancing
WO3, 3 Layers
V2O5, 3 Layers
Current Density (μA/cm2)
Time (s)
Reduction
4 – 2.1 V (vs. Li/Li+)
(0.1 mV/s)
1
0
-1
-2
-3
-4
-5
0
5000
10000
15000

**Figure S4**

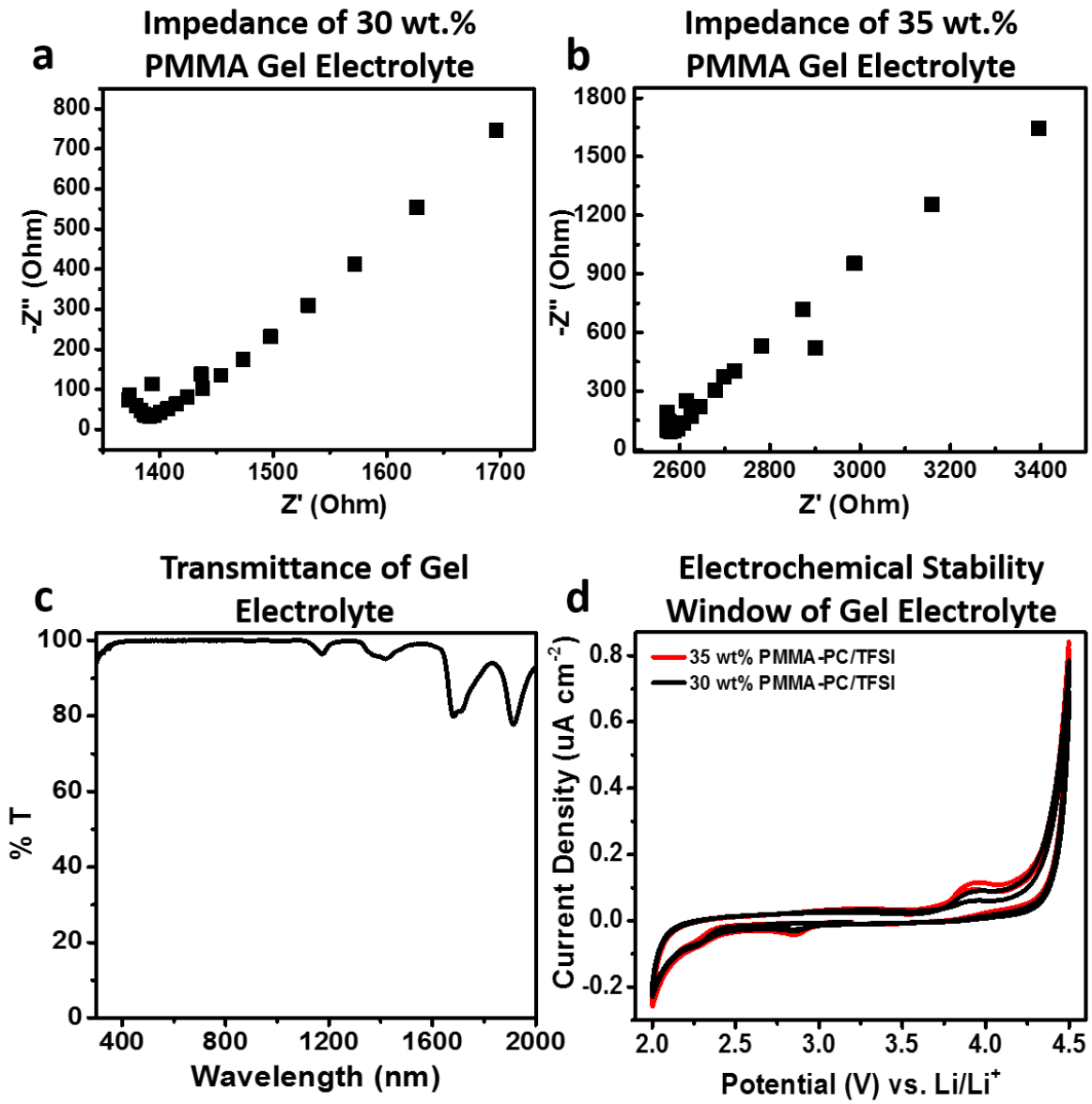
a
Impedance of 30 wt.% PMMA Gel Electrolyte
-Z'' (Ohm)
Z' (Ohm)
b
Impedance of 35 wt.% PMMA Gel Electrolyte
-Z'' (Ohm)
Z' (Ohm)
c
Transmittance of Gel Electrolyte
% T
Wavelength (nm)
d
Electrochemical Stability Window of Gel Electrolyte
35 wt% PMMA-PC/TFSI
30 wt% PMMA-PC/TFSI
Current Density (uA cm-2)
Potential (V) vs. Li/Li+

**Figure S5**

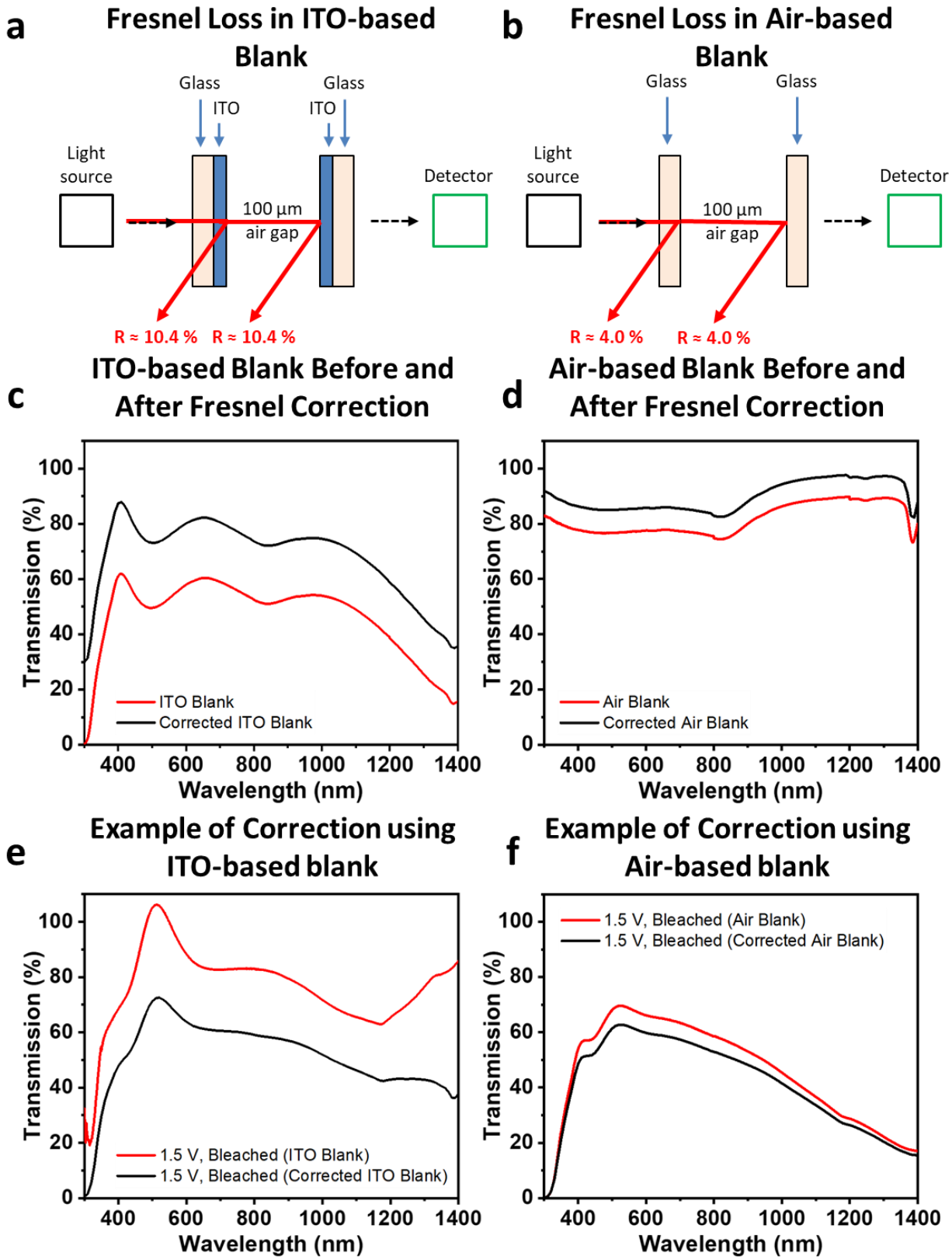
a
Fresnel Loss in ITO-based Blank
Glass
ITO
Glass
ITO
Light source
100 µm air gap
Detector
R ≈ 10.4 %
R ≈ 10.4 %
b
Fresnel Loss in Air-based Blank
Glass
Glass
Light source
100 µm air gap
Detector
R ≈ 4.0 %
R ≈ 4.0 %
c
ITO-based Blank Before and After Fresnel Correction
Transmission (%)
Wavelength (nm)
ITO Blank
Corrected ITO Blank
d
Air-based Blank Before and After Fresnel Correction
Transmission (%)
Wavelength (nm)
Air Blank
Corrected Air Blank
e
Example of Correction using ITO-based blank
Transmission (%)
Wavelength (nm)
1.5 V, Bleached (ITO Blank)
1.5 V, Bleached (Corrected ITO Blank)
f
Example of Correction using Air-based blank
Transmission (%)
Wavelength (nm)
1.5 V, Bleached (Air Blank)
1.5 V, Bleached (Corrected Air Blank)

**Figure S6**

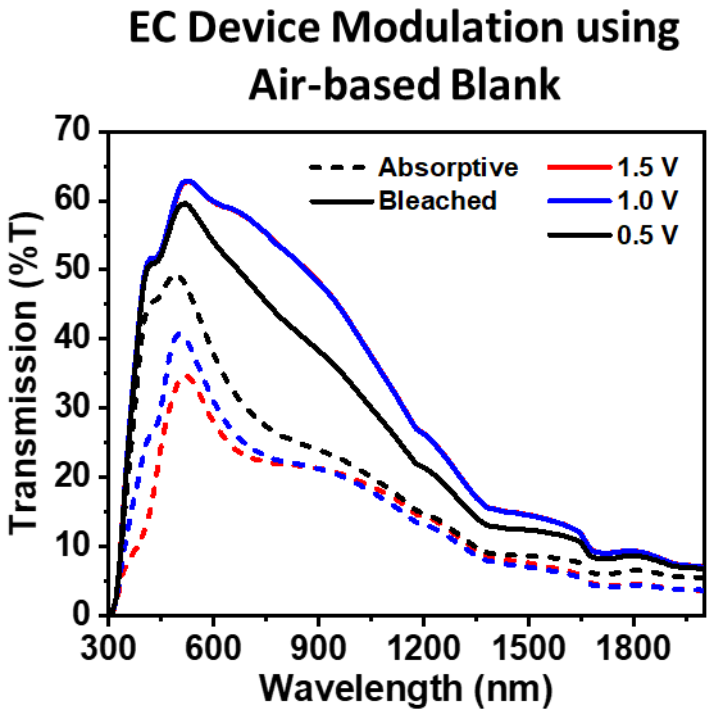
EC Device Modulation using
Air-based Blank
Absorptive
Bleached
1.5 V
1.0 V
0.5 V
Transmission (%T)
Wavelength (nm)
0
10
20
30
40
50
60
70
300
600
900
1200
1500
1800

**Figure S7**

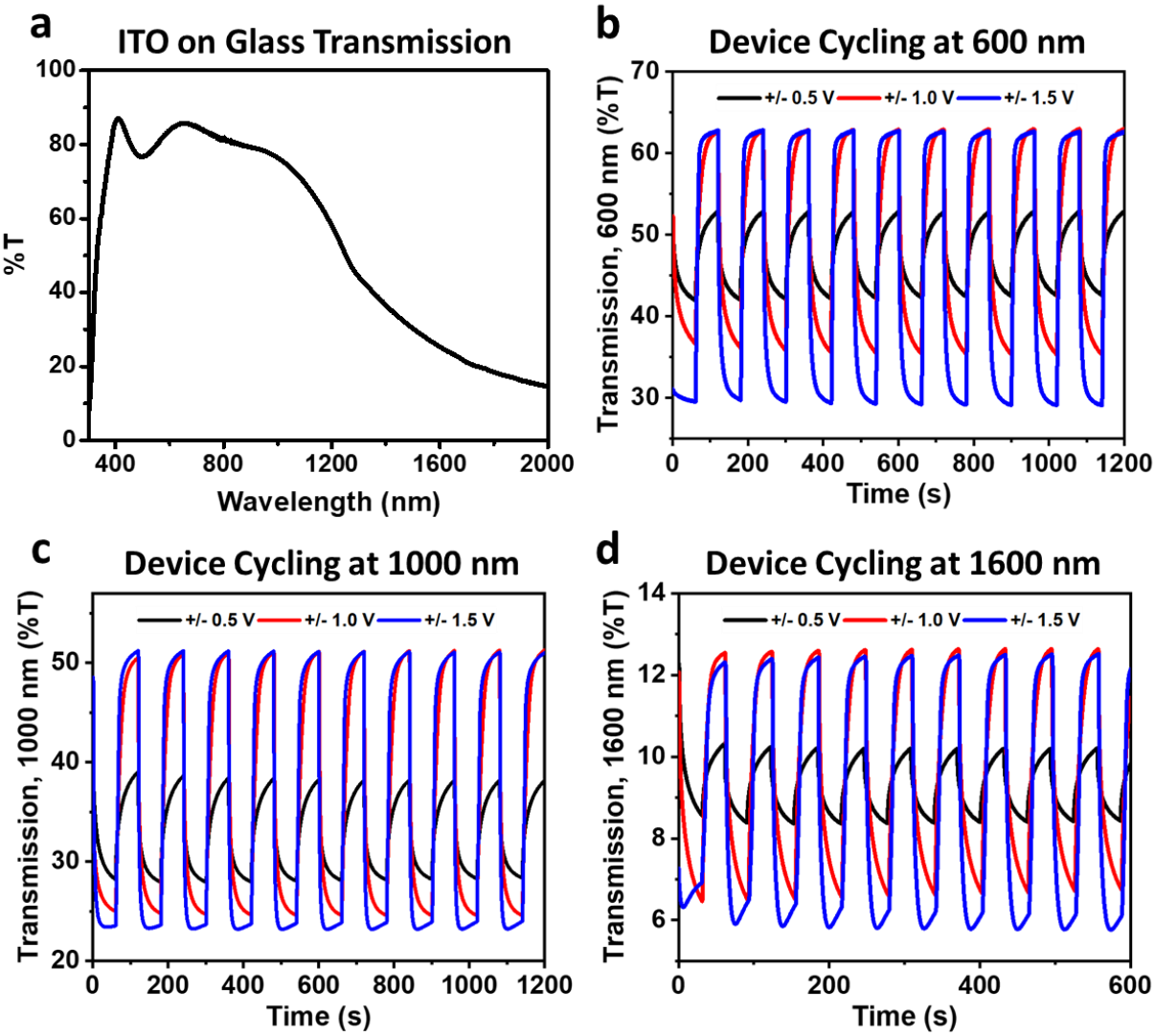
a
ITO on Glass Transmission
%T
Wavelength (nm)
b
Device Cycling at 600 nm
+/- 0.5 V
+/- 1.0 V
+/- 1.5 V
Transmission, 600 nm (%T)
Time (s)
c
Device Cycling at 1000 nm
+/- 0.5 V
+/- 1.0 V
+/- 1.5 V
Transmission, 1000 nm (%T)
Time (s)
d
Device Cycling at 1600 nm
+/- 0.5 V
+/- 1.0 V
+/- 1.5 V
Transmission, 1600 nm (%T)
Time (s)

**Figure S8**

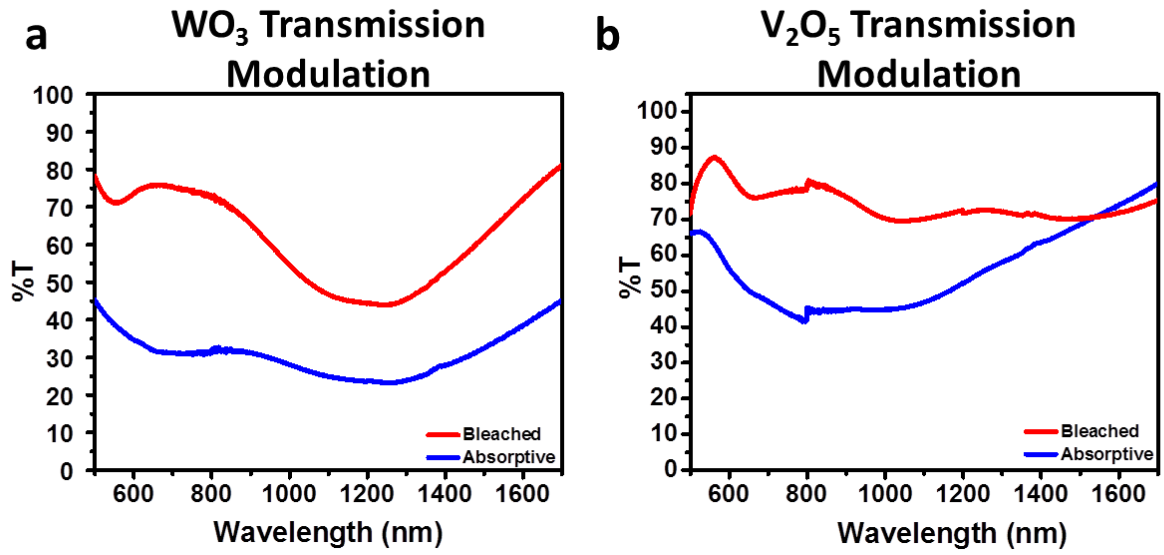
a
WO3 Transmission Modulation
%T
Wavelength (nm)
Bleached
Absorptive
b
V2O5 Transmission Modulation
%T
Wavelength (nm)
Bleached
Absorptive

**Figure S9**

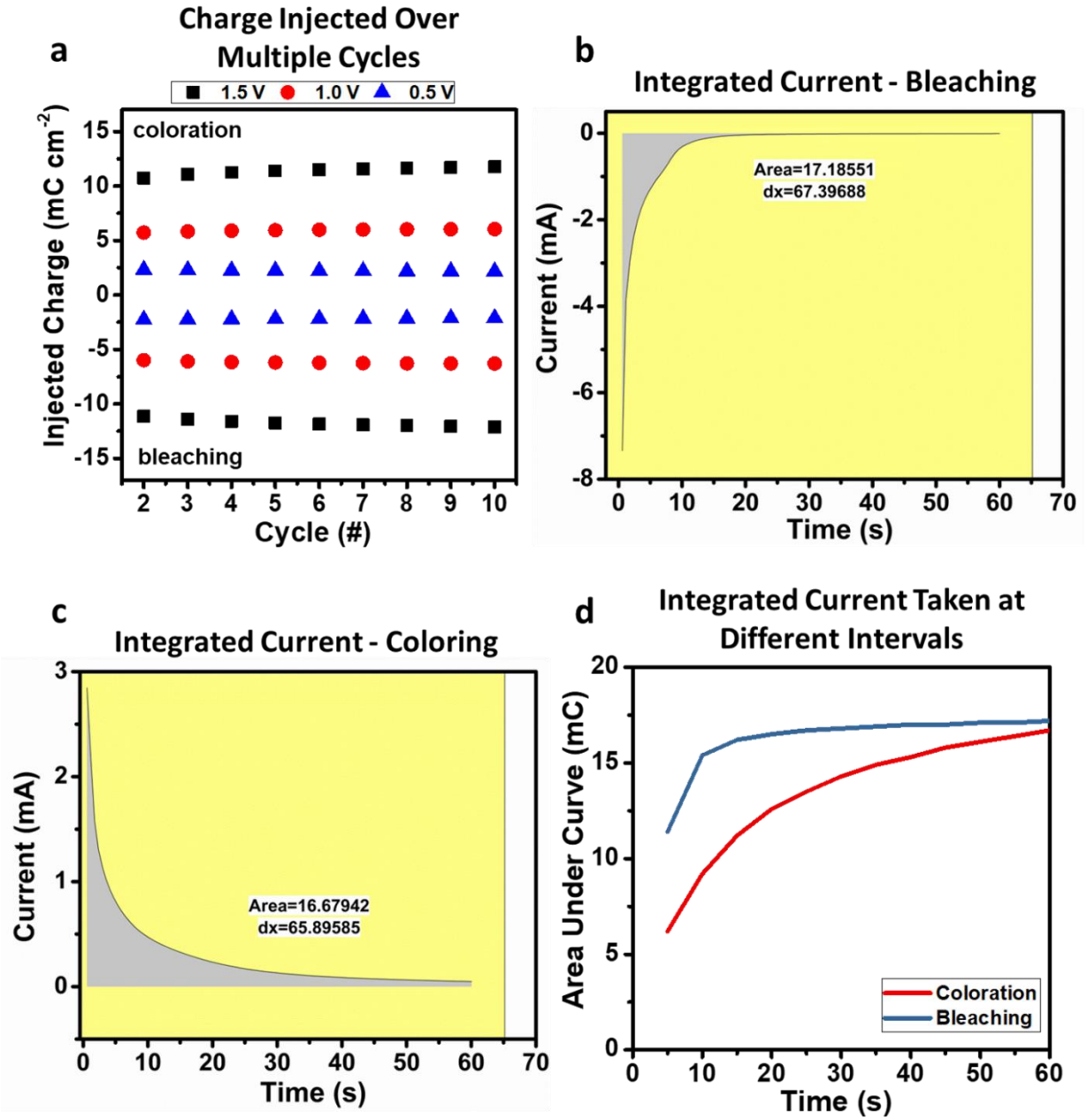
a
Charge Injected Over Multiple Cycles
1.5 V
1.0 V
0.5 V
coloration
bleaching
Injected Charge (mC cm-2)
Cycle (#)
b
Integrated Current - Bleaching
Area=17.18551
dx=67.39688
Current (mA)
Time (s)
c
Integrated Current - Coloring
Area=16.67942
dx=65.89585
Current (mA)
Time (s)
d
Integrated Current Taken at Different Intervals
Area Under Curve (mC)
Coloration
Bleaching
Time (s)

**Figure S10**

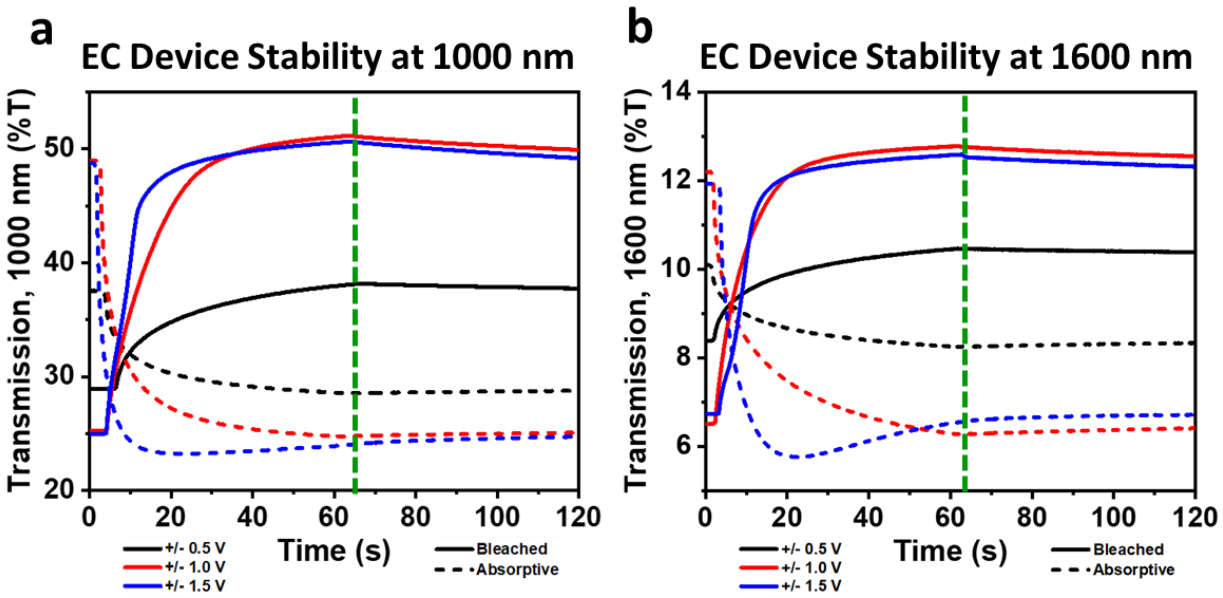
a
EC Device Stability at 1000 nm
Transmission, 1000 nm (%T)
Time (s)
+/- 0.5 V
+/- 1.0 V
+/- 1.5 V
Bleached
Absorptive
b
EC Device Stability at 1600 nm
Transmission, 1600 nm (%T)
Time (s)
+/- 0.5 V
+/- 1.0 V
+/- 1.5 V
Bleached
Absorptive

**Figure S11**

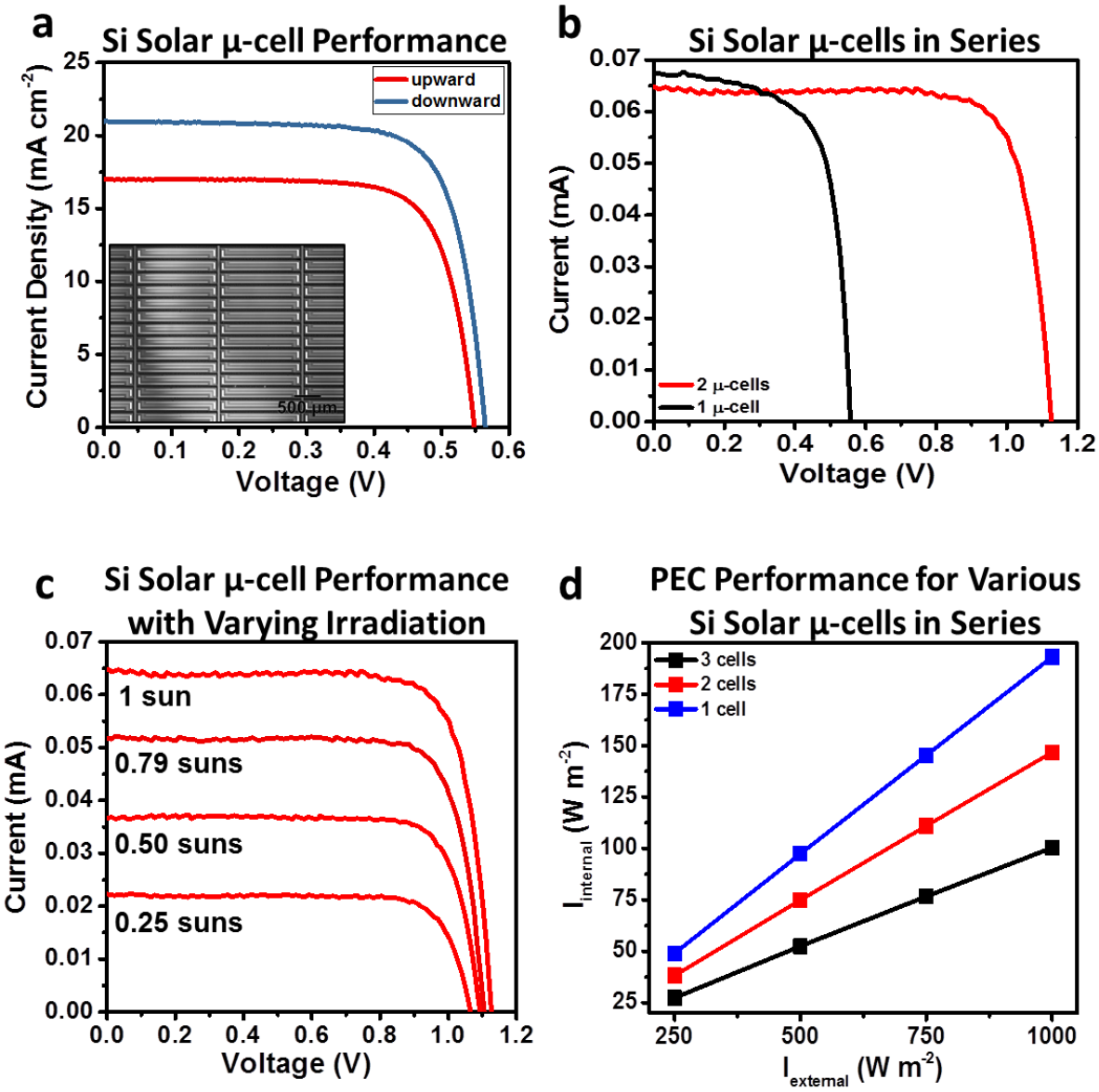
a
Si Solar µ-cell Performance
upward
downward
Current Density (mA cm-2)
Voltage (V)
500 µm
b
Si Solar µ-cells in Series
Current (mA)
2 µ-cells
1 µ-cell
Voltage (V)
c
Si Solar µ-cell Performance with Varying Irradiation
1 sun
0.79 suns
0.50 suns
0.25 suns
Current (mA)
Voltage (V)
d
PEC Performance for Various Si Solar µ-cells in Series
3 cells
2 cells
1 cell
I internal (W m-2)
I external (W m-2)

**Figure S12**

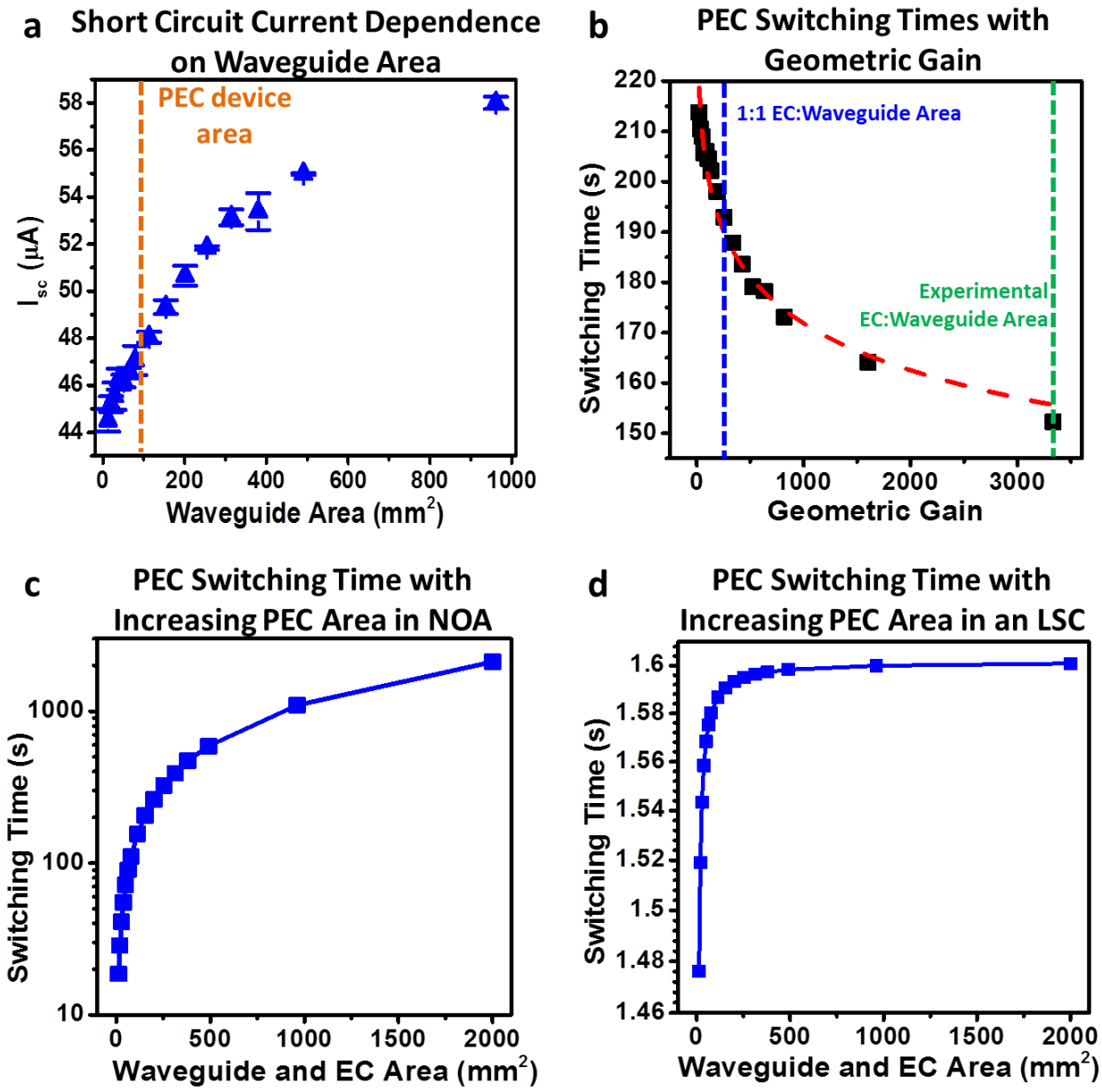
a
Short Circuit Current Dependence on Waveguide Area
PEC device area
$I_{sc}$ (μA)
Waveguide Area (mm$^2$)
b
PEC Switching Times with Geometric Gain
1:1 EC:Waveguide Area
Experimental EC:Waveguide Area
Switching Time (s)
Geometric Gain
c
PEC Switching Time with Increasing PEC Area in NOA
Switching Time (s)
Waveguide and EC Area (mm$^2$)
d
PEC Switching Time with Increasing PEC Area in an LSC
Switching Time (s)
Waveguide and EC Area (mm$^2$)

**Figure S13**

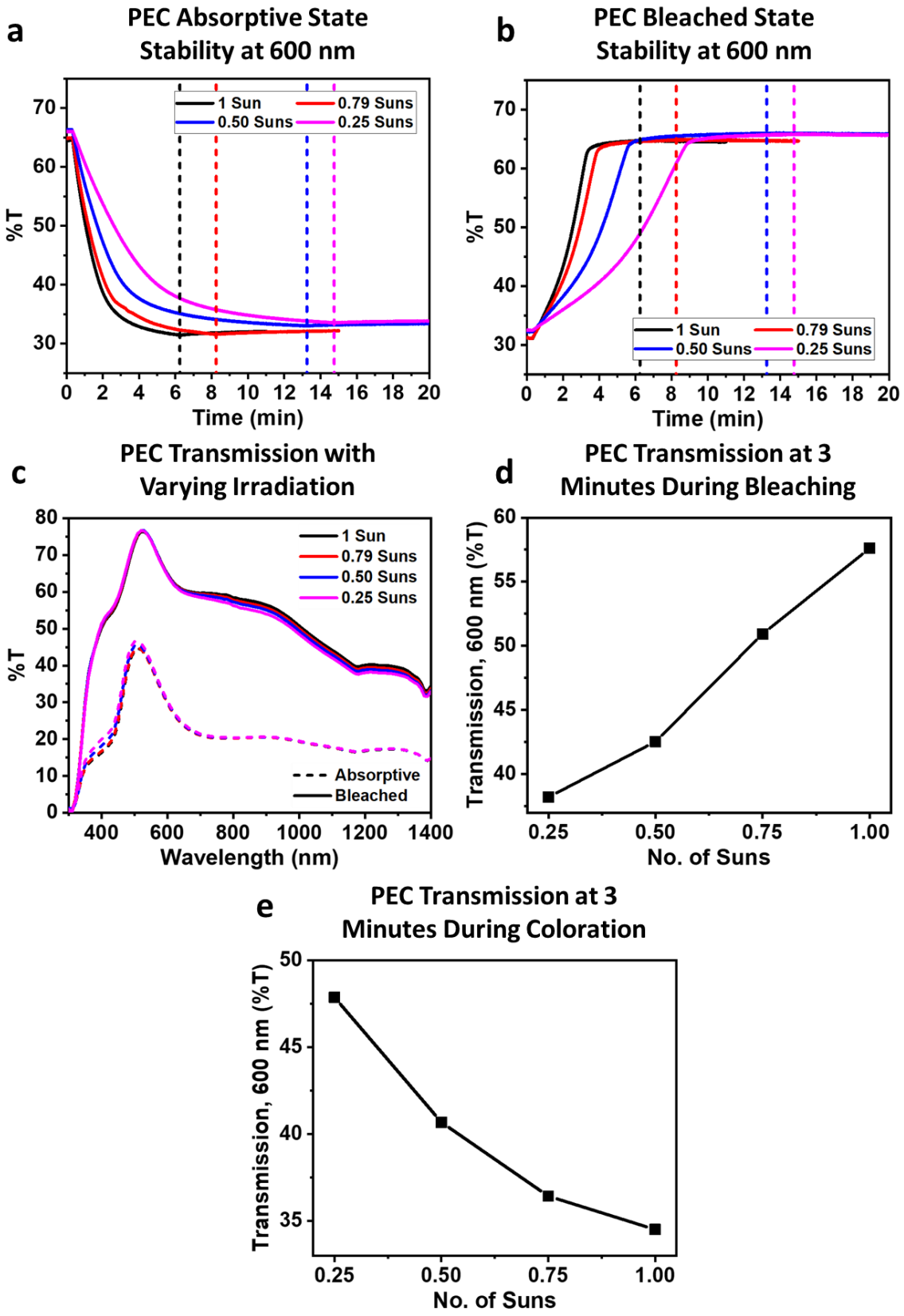
a
PEC Absorptive State Stability at 600 nm
1 Sun
0.79 Suns
0.50 Suns
0.25 Suns
%T
Time (min)
b
PEC Bleached State Stability at 600 nm
1 Sun
0.79 Suns
0.50 Suns
0.25 Suns
%T
Time (min)
c
PEC Transmission with Varying Irradiation
1 Sun
0.79 Suns
0.50 Suns
0.25 Suns
Absorptive
Bleached
%T
Wavelength (nm)
d
PEC Transmission at 3 Minutes During Bleaching
Transmission, 600 nm (%T)
No. of Suns
e
PEC Transmission at 3 Minutes During Coloration
Transmission, 600 nm (%T)
No. of Suns

**Figure S14**

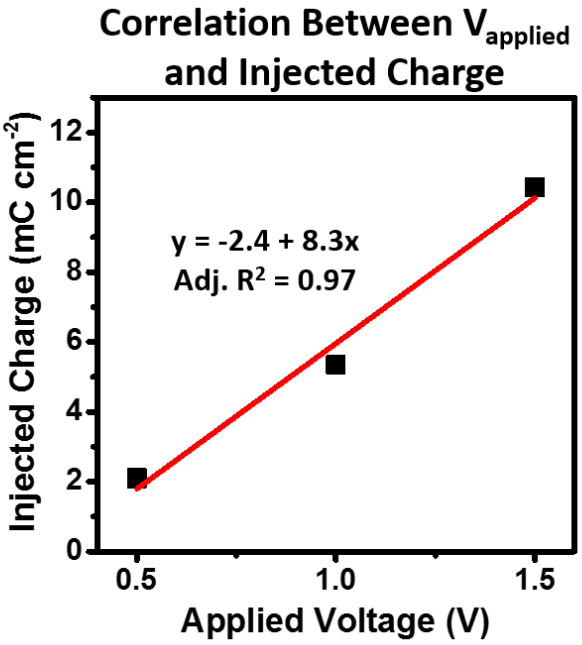
Correlation Between $V_{applied}$ and Injected Charge
Injected Charge (mC cm$^{-2}$)
0
2
4
6
8
10
12
y = -2.4 + 8.3x
Adj. $R^2$ = 0.97
0.5
1.0
1.5
Applied Voltage (V)

**Figure S15**

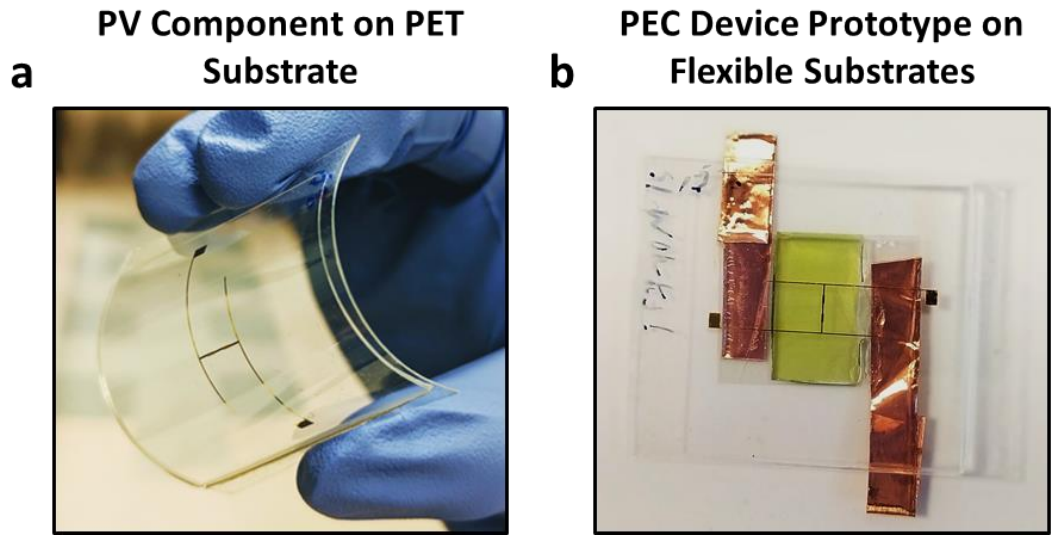
a
PV Component on PET Substrate
b
PEC Device Prototype on Flexible Substrates

**Figure S16**

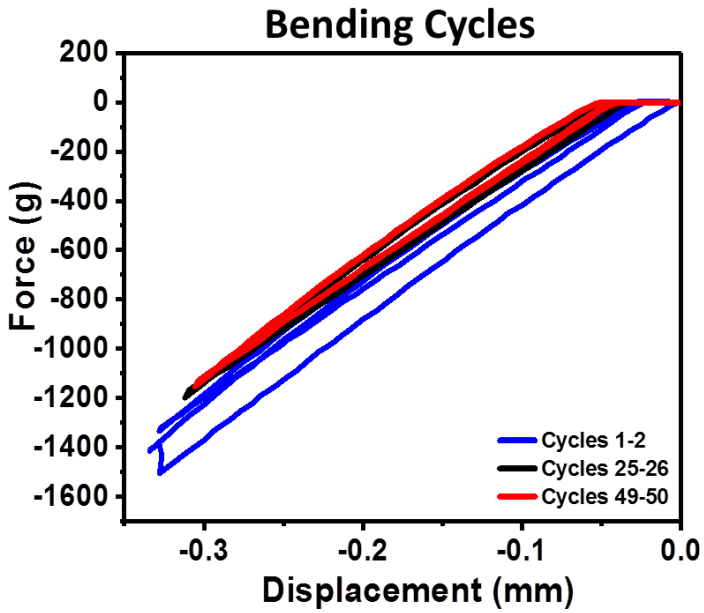
Bending Cycles
200
0
-200
-400
-600
-800
-1000
-1200
-1400
-1600
Force (g)
-0.3
-0.2
-0.1
0.0
Displacement (mm)
Cycles 1-2
Cycles 25-26
Cycles 49-50